Sensors & Diagnostics

PAPER

View Article Online
View Journal | View Issue

Open Access Article. Published on 21 November 2023. Downloaded on 1/13/2026 2:05:29 AM.
This article is licensed under a Creative Commons Attribution-NonCommercial 3.0 Unported Licence.

Check for updates

Cite this: *Sens. Diagn.*, 2024, **3**, 269

Vertically-grown Ag nanoplates on $SeZnO_3$ nanosheets for an enhanced pressure sensing performance†

Zeyi Wang, Yuping Li, Jian Zhang* and Xiao Huang *

Received 31st May 2023,
Accepted 20th November 2023

DOI: 10.1039/d3sd00130j

rsc.li/sensors

As a piezoelectric ceramic material, $SeZnO_3$ has received increasing attention for pressure sensing. However, the poor conductivity and low dielectric constant of bare $SeZnO_3$ severely limit its wide applications. Herein, to improve the pressure sensing properties of $SeZnO_3$, $SeZnO_3$ nanosheets composited with Ag nanoplates were synthesized *via* a dissolution coprecipitation method, which exhibited a higher sensitivity (54.8 kPa^{-1}) to external pressure with an excellent repeatability than that of bare $SeZnO_3$ nanosheets (12.3 kPa^{-1}). The enhanced pressure sensing properties of Ag/$SeZnO_3$ nanocomposites could be attributed to an increased dielectric constant and an enhanced charge output. Moreover, the nanocomposite-based pressure sensors showed an accelerated response/recovery rate (0.7 s/2.7 s) because of the effective charge transfer between $SnZnO_3$ and Ag, which was confirmed by XPS results. This Ag/$SeZnO_3$ composite nanosheet-based pressure sensor demonstrates a potential for practical monitoring of human movement.

1. Introduction

Pressure sensors have received significant attention, showing widespread potential applications in wearable sensing devices,[1] electronic skins (e-skins),[2] and healthcare detection.[3] To date, several sensing mechanisms have been employed for the fabrication of pressure sensors, including piezoresistive,[4] capacitance,[5] and piezoelectric[6] sensing. Among them, capacitance-type pressure sensors with the advantages of a simple device structure, long-term stability, low power consumption, high sensitivity, and fast response have received special attention.[7,8] In such types of devices, a dielectric sensing layer is commonly sandwiched between two parallel plate electrodes. It is believed that a higher dielectric constant and material stability are the prerequisites for the achievement of higher pressure-sensing properties.[9–12]

As a type of perovskite-type ceramic oxide, $SeZnO_3$ has attracted increasing attention for pressure sensing applications due to its special crystal structure,[13] large surface area, and abundant oxygen vacancies.[14] $SeZnO_3$ is a rare perovskite oxide with a valence combination of $Se^{4+}Zn^{2+}$-O_3. The theoretical calculation results revealed that $SeZnO_3$ showed a ductile nature with excellent mechanical properties, exhibiting potential applications in pressure sensing.[15] However, because of its poor conductivity and low dielectric constant, the research on $SeZnO_3$-based pressure sensors is still in its infancy. Therefore, it is expected that the modulation of conductivity and dielectric constant can be helpful for the improvement of its pressure sensing properties. It was reported that the surface modification of noble metal nanoparticles, such as Ag, Au, and Pd,[16] on pressure sensing materials can improve their electrical conductivity[17] and dielectric constant.[18] Among them, Ag nanoparticles are widely adopted as surface modification materials because of their low cost, simple preparation, high dielectric constant,[19] and good conductivity.[20] However, the modification of Ag nanoparticles with a uniform distribution and controllable morphological structure is still challenging.

Herein, $SeZnO_3$ nanosheets were firstly synthesized *via* a dissolution coprecipitation method. Next, $SeZnO_3$ nanosheets decorated with Ag nanoparticles were successfully prepared using a facile photo-reduction method. Moreover, by tuning the concentration of $AgNO_3$, the morphological structure of Ag could be adjusted. The pressure-sensing results revealed that the Ag/$SeZnO_3$ composite showed a higher sensitivity and faster response/recovery rate compared to the bare $SeZnO_3$ nanosheets, which is attributed to its increased dielectric constant and enhanced charge output.

2. Experiments

2.1 Materials

Sodium selenite (Na_2SeO_3, >98%) was purchased from Shanghai Adamas Reagent Co. Ltd., China. Sodium dodecyl

Institute of Advanced Materials (IAM), School of Flexible Electronics (SoFE), Jiangsu National Synergetic Innovation Center for Advanced Materials (SICAM), Nanjing Tech University (Nanjing Tech), 30 South Puzhu Road, Nanjing 211816, China. E-mail: iamjzhang@njtech.edu.cn, iamxhuang@njtech.edu.cn

† Electronic supplementary information (ESI) available. See DOI: https://doi.org/10.1039/d3sd00130j

Open Access Article. Published on 21 November 2023. Downloaded on 1/13/2026 2:05:29 AM.
This article is licensed under a Creative Commons Attribution-NonCommercial 3.0 Unported Licence.

sulfonate (SDS, >99.7%) was purchased from Shanghai Lingfeng Chemical Reagent Co. Ltd., China. Silver nitrate ($AgNO_3$, >99.7%) was purchased from Shanghai Aladdin Technology Co., Ltd., China. Zinc chloride anhydrous ($ZnCl_2$, >99.7%), ethanol (anhydrous, >99.7%), and ethanediol (anhydrous, >99.7%) were purchased from Sinopharm Chemical Reagent Co., Ltd., China. Deionized (DI) water was purified using a Milli-Q System (Millipore). All materials were used without further purification.

2.2 Synthesis of $SeZnO_3$ nanoplates and Ag nanosheets/$SeZnO_3$ nanoplates

$SeZnO_3{\cdot}H_2O$ was synthesized *via* the dissolution coprecipitation method. Briefly, 0.4 g Na_2SeO_3 was dissolved in 10 mL DI water, followed by the addition of 0.9 g SDS. The mixed solution was stirred at 1500 rpm for 30 min, and then sonicated at 25 °C for 30 min to remove bubbles. The as-obtained viscous solution was added dropwise to a 0.01 M $ZnCl_2$ aqueous solution under constant stirring at 1500 rpm for 30 min, and then transferred to an oven at 90 °C for 1 h. The resulting precipitate was collected by centrifugation and washed several times with DI water and ethanol. Finally, the washed precipitate was dried overnight at 70 °C and $SeZnO_3{\cdot}H_2O$ nanosheets were obtained. To remove the crystal water of $SeZnO_3{\cdot}H_2O$, it was transferred to a tubular furnace and heated for 3 h under an air atmosphere at 400 °C.

Ag/$SeZnO_3$ was synthesized *via* the photo-reduction method. Briefly, 0.09 g $AgNO_3$ was added to 3 mL ethanediol. The mixture was sonicated for 15 min, and then 0.046 mg $SeZnO_3$ was added under constant stirring at 1000 rpm for 30 min. The mixed solution was irradiated by a 150 W Xenon lamp for 30 min. The products were collected by centrifugation and washed several times with ethanol.

2.3 Apparatus and measurements

The as-prepared samples were characterized *via* scanning electron microscopy (SEM JEOL JSM-7800F, Japan), transmission electron microscopy (TEM JEOL 2100 F, Japan), high-resolution transmission electron microscopy (HRTEM JEOL 2100 Plus, Japan), X-ray diffraction (XRD, Smart Lab Rigaku, Japan) with Cu Kα radiation at λ = 1.54 Å, X-ray photoelectron spectroscopy (XPS, Versaprobe PHI 5000, Japan) and LCR digital electric bridge (Honghui TH26011BS, China). The dielectric constant was tested using a precision digital electric bridge (Agilent 4980A, USA).

2.4 Fabrication and test of pressure sensors

Briefly, 200 μL of dispersed $SeZnO_3$ or Ag/$SeZnO_3$ ethanol solution was dropped on coper tape (1 × 1 cm^2). After the evaporation of ethanol, another layer of copper tape was covered on it to obtain the pressure sensing devices.

The abovementioned sensing devices were connected to an LCR. During the pressure testing, the starting pressure was set as 0 Pa (without loading extra pressure), and a target pressure was applied to the sensor with a 15 s holding time. The testing pressure was in the range of 34.8 Pa to 1240 Pa.

3. Results and discussion

Fig. 1a shows a schematic diagram of the process for the preparation of the Ag–$SeZnO_3$ nanocomposite. Firstly, bare $SnZnO_3$ nanosheets were prepared *via* the dissolution coprecipitation method with Na_2SeO_3, SDS, and $ZnCl_2$ as precursors. Subsequently, the Ag/$SeZnO_3$ composite nanosheets were prepared by air annealing, followed by the photo-reduction method. As shown in Fig. 1b, well-defined XRD peaks assigned to the (111), (112), (004), (211), and (213) planes of $SeZnO_3$ (JCPDS No. 78-0446) can be clearly observed, indicating that $SeZnO_3$ was successfully prepared. It can be found from the transmission electron microscopy (TEM) images (Fig. 1c) that the as-prepared $SeZnO_3$ nanosheets exhibited a two-dimensional (2D) structure (transverse size = 1–2 μm) with a uniformly distributed pore structure on their surface. The elemental distribution of the $SeZnO_3$ nanosheets was analyzed by energy-dispersive X-ray spectroscopy (EDS) mapping (Fig. S1†), which showed the uniform distribution of Se and Zn in the $SeZnO_3$ nanosheets, and the stoichiometric ratio of Se : Zn : O in the $SeZnO_3$ nanosheets was around 1 : 1 : 3. The crystal structure of the $SeZnO_3$ nanosheets was further investigated by high-resolution TEM (HRTEM) (Fig. 1d), which showed interplanar distances of 0.25 nm and 0.31 nm, corresponding to the (114) and (120) crystal planes of the $SeZnO_3$ nanosheets, respectively. In the case of the Ag/$SeZnO_3$ nanocomposite, not only the diffraction peak of $SeZnO_3$ could be observed, but an extra peak assigned to the (111) plane of Ag (JCPDS No. 04-0783) clearly found, as shown in Fig. 1e, which suggests that Ag/$SeZnO_3$ was successfully prepared. Similarly,

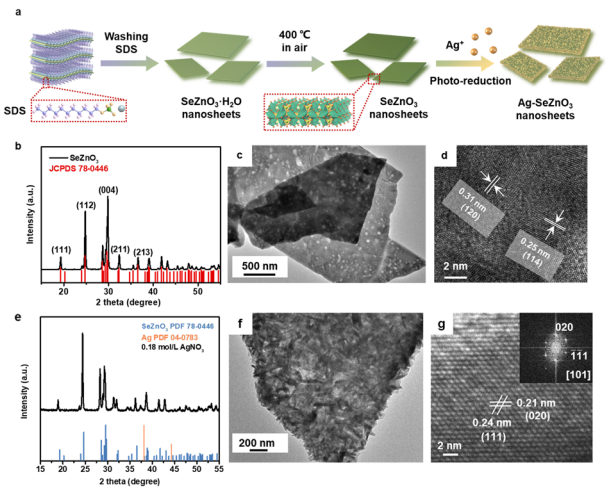

Fig. 1 (a) A schematic diagram of the synthesis of $SeZnO_3$ nanosheets. (b) The XRD patterns of $SeZnO_3$ nanosheets. (c) The TEM image of $SeZnO_3$ nanosheets. (d) The HRTEM image of $SeZnO_3$ nanosheets. (e) The XRD patterns of Ag/$SeZnO_3$ nanosheets. (f) The TEM image of Ag/$SeZnO_3$ nanosheets. (g) The HRTEM image of Ag/$SeZnO_3$ nanosheets (inset: the fast Fourier transform (FFT) pattern of the HRTEM image).

 © 2024 The Author(s). Published by the Royal Society of Chemistry

Open Access Article. Published on 21 November 2023. Downloaded on 1/13/2026 2:05:29 AM.
This article is licensed under a Creative Commons Attribution-NonCommercial 3.0 Unported Licence.

the Ag/$SeZnO_3$ nanosheets also exhibited a 2D structure with an undamaged profile structure compared to the bare $SeZnO_3$ nanosheet structure (Fig. 1f). Interestingly, it was found that Ag nanoplates were grown vertically on the surface of the $SeZnO_3$ nanosheets. The elemental distribution in the Ag/$SeZnO_3$ nanosheets was also analysed by EDS mapping (Fig. S2†), which showed the uniform distribution of Ag on the $SeZnO_3$ nanosheet with an Se : Zn : Ag ratio of 1 : 1 : 1, further indicating the successful preparation of Ag/$SeZnO_3$. The crystal structure of the Ag/$SeZnO_3$ nanosheets was also investigated by HRTEM (Fig. 1d), which showed interplanar distances of 0.21 nm and 0.24 nm, corresponding to the (020) and ($\bar{1}\bar{1}1$) crystal planes of Ag, respectively.

To further study the structure and phase evolution, the chemical composition and chemical bonding states of the as-prepared $SeZnO_3$ and Ag/$SeZnO_3$ nanocomposite were confirmed by XPS characterization. Fig. 2a shows the Se 3d XPS spectrum, which could be deconvoluted into two peaks (Se $3d_{5/2}$ and Se $3d_{3/2}$) at 58.7 and 59.2 eV, respectively, corresponding to the SeO_3^{2-} state (Se–O binding structure of $SeZnO_3$).[21] It should be noted that the binding energy of Se 3d in the nanocomposite shifted towards a lower binging energy compared to the bare $SeZnO_3$, owing to the weaker electronegativity of Ag compared to Se. The binding energy shift indicates the effective electron transfer between the $SeZnO_3$ nanosheets and Ag nanoplates. In the Zn 2p spectra of $SeZnO_3$ and Ag/$SeZnO_3$ (Fig. 2b), the two peaks corresponding to Zn $2p_{1/2}$ and Zn $2p_{3/2}$ are located at 1044.8 eV and 1021.7 eV, respectively. The difference in the binding energy of these two peaks suggests that the Zn species was the Zn^{2+} state (Zn–O binding structure of $SeZnO_3$).[22] The O 1s XPS spectrum in Fig. 2c could be deconvoluted into two peaks, which are located at 530.6 and 531.3 eV, corresponding to lattice oxygen and oxygen vacancy, respectively. The peak assigned to lattice oxygen matched well with the above-mentioned Se 3d and Zn 2p spectra, further confirming the existence of Se–O (A site of $SeZnO_3$) and Zn–O (B site of $SeZnO_3$) in the $SeZnO_3$ structure.[23,24] In addition, the extra Ag 3d spectrum of the nanocomposite showed two peaks at 368.19 eV (Ag $3d_{5/2}$) and 374.19 (Ag $3d_{3/2}$), which can be assigned to the Ag^0 state, further proving that Ag^+ was successfully reduced to Ag^0 by the photo-reduction method.[25]

Besides, to detail the effect of Ag on the morphological structure and the pressure sensing properties of the nanocomposite, the concentration of $AgNO_3$ was also tuned, while keeping the other synthesis conditions unchanged. It was found that the morphological structure of Ag changed from nanoparticles to nanoplates (Fig. S3†) when increasing the $AgNO_3$ concentration from 0.03 and 0.06 to 0.18 mol L^{-1}. Moreover, the XRD patterns of the nanocomposites with different concentrations of $AgNO_3$ are presented in Fig. S4,† all of which matched well with the (111), (112), (004), (211), and (213) planes of $SeZnO_3$ (JCPDS No. 78-0446) and (111) plane of Ag (JCPDS No. 04-0783).

As a demonstration, the bare $SeZnO_3$ and Ag/$SeZnO_3$ nanocomposites with different contents of Ag were fabricated into pressure sensors to measure pressures in the range of 34.8 Pa to 1240 Pa (Fig. 3a). The sensor response was defined by $(C_p - C_0)/C_0$%, where C_0 is the initial capacitance and C_p is the capacitance under external pressure. The response of the Ag/$SeZnO_3$-based pressure sensor in the whole pressure range was higher than that of the $SeZnO_3$-based pressure sensor. Moreover, with an increase in the $AgNO_3$ concentration from 0.03 and 0.06 to 0.18 mol L^{-1}, the responses of the nanocomposite also increased accordingly. The fitted pressure-response curves for the different pressure

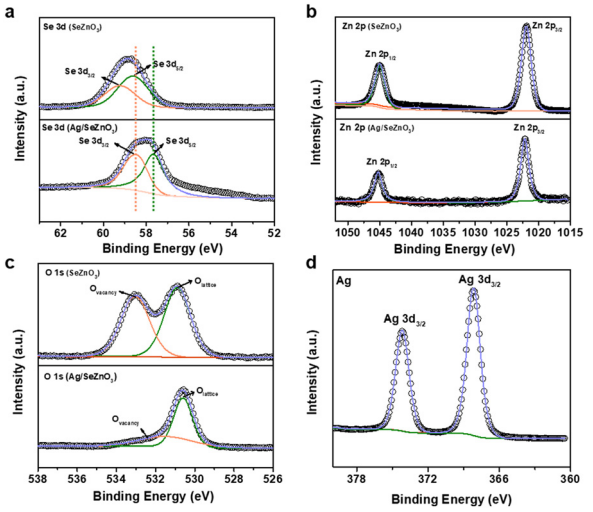

Fig. 2 The XPS spectra of (a) Se 3d, (b) Zn 2p, and (c) O 1s of $SeZnO_3$ nanosheets and Ag/$SeZnO_3$ nanosheets and (d) Ag 3d of Ag/$SeZnO_3$ nanosheets. The inserted dash lines can be used to determine the shift directions of the identified peaks.

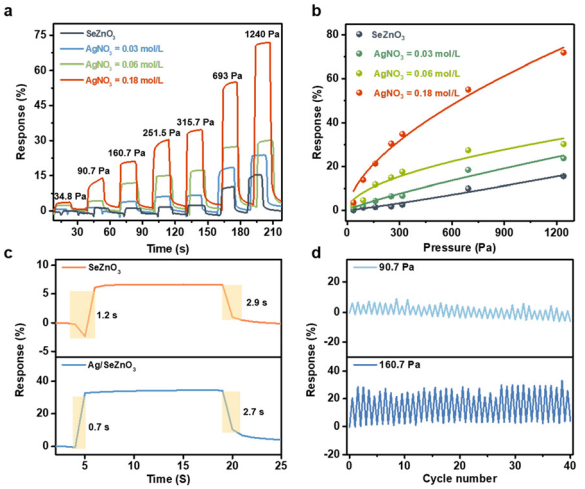

Fig. 3 (a) The response and recovery curves of the pressure sensors based on $SeZnO_3$ and Ag/$SeZnO_3$ nanosheets. (b) The pressure-response curves of sensors based on $SeZnO_3$ and Ag/$SeZnO_3$ nanosheets. (c) The response and recovery time of pressure sensors based on $SeZnO_3$ and Ag/$SeZnO_3$ nanosheets under 251.5 Pa. (d) The long-term stability of sensor based on $BiFeO_3$ nanoplates under 90.7 Pa and 160.7 Pa pressure.

Open Access Article. Published on 21 November 2023. Downloaded on 1/13/2026 2:05:29 AM.
This article is licensed under a Creative Commons Attribution-NonCommercial 3.0 Unported Licence.

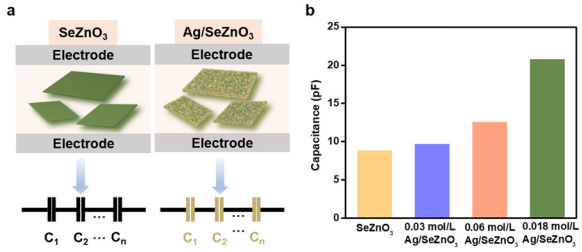

Fig. 4 (a) A schematic illustration of $SeZnO_3$- and Ag/$SeZnO_3$-based pressure sensors. (b) The capacitance outputs of $SeZnO_3$- and Ag/$SeZnO_3$-based pressure sensors with different concentrations of Ag loading.

sensors are shown in Fig. 3b. The sensitivity of these pressure sensors was calculated as follows:

$$\text{Sensitivity} = [(C_t - C_0)/C_0 \times 100\%]/\Delta P \quad (1)$$

where ΔP is the variation in pressure. The sensitivity of Ag/$SeZnO_3$ with 0.06, 0.06 and 0.18 mol L^{-1} $AgNO_3$ concentration was 23.2, 27.2 and 54.8 kPa^{-1}, respectively, while that of the bare $SeZnO_3$ is only 18.2 kPa^{-1}. Fig. 3c shows the dynamic response-recovery curves of the Ag/$SeZnO_3$ (0.18 mol L^{-1}) and bare $SeZnO_3$-based sensors to 251.5 Pa. Interestingly, the Ag/$SeZnO_3$ (0.18 mol L^{-1})-based pressure sensor showed a shorter response and recovery time (0.7 s/2.7 s) than that of the bare $SeZnO_3$-based pressure sensor (1.2 s/2.9 s). Besides, the durability of our sensor based on Ag/$SeZnO_3$ nanosheets was evaluated by sensing tests under repeated loading of 90.7 Pa and 160.7 Pa pressure. As shown in Fig. 3d, the sensor exhibited stable sensing responses without obvious degradation after 40 cycles, suggesting its good stability.

To detail the enhanced pressure sensitivity of the nanocomposite, the equivalent circuit model based on the bare $SnZnO_3$ and Ag/$SnZnO_3$ nanocomposite were constructed. The whole capacitance of the as-fabricated sensors can be divided into many "mini capacitors". As shown in Fig. 4a, it is believed that the number of electric connections between the bare $SeZnO_3$ and electrodes is smaller than that of the Ag/$SeZnO_3$ nanocomposites due to the decoration of Ag nanoplates with more contact sites. Therefore, the introduction of Ag nanoparticles can provide more electric connection between sensing materials and electrodes, leading to an increase in the series capacitance in nanocomposites-based pressure sensors. To further confirm the higher capacitance of the nanocomposite, the relative permittivity of the Ag/$SeZnO_3$ nanosheets and bare $SeZnO_3$ was also calculated, which was 119.29 and 33.63, respectively. According to the definition of capacitance, a higher permittivity implies a higher output capacitance, which is consistent with the experimental capacitance values. As shown in Fig. 4b, the initial capacitance of the nanocomposite increased with an increase in Ag concentration, which could increase the signal-to-noise ratio (SNR) of the pressure sensor and increase the measurement accuracy.[26] Besides, according to the enhanced electrical conductivity of the nanocomposite, its electron density also increased with an increase in the Ag loading, which is beneficial for an enhancement in pressure sensitivity. The higher output capacitance of the nanocomposites can be helpful for the enhancement of pressure sensitivity.[27] Besides, it was reported that the addition of Ag nanoparticles can enlarge the deformation of the sensing layer under external pressure, leading to the enhanced pressure sensitivity of the nanocomposite. Because of the effective electron transfer between Ag and $SeZnO_3$ and the higher conductivity of Ag, the pressure-induced charge generation can be easily collected, leading to the fast response/recovery rate of the Ag/$SeZnO_3$ nanocomposites.

4. Conclusions

In summary, $SeZnO_3$ nanosheets composited with Ag nanoparticles were successfully prepared *via* the dissolution coprecipitation method, followed by photoreduction, which exhibited enhanced pressure sensitivity with excellent repeatability compared to that of bare $SeZnO_3$ nanosheets. With an increase in the concentration of $AgNO_3$, the morphological structure of Ag could be tuned from nanoparticles to nanoplates. Moreover, the pressure sensitivity of the nanocomposite also increased with an increase in the amount of Ag. It is believed that the increased dielectric constant-induced higher output capacitance was beneficial for the higher sensitivity of the nanocomposite. Because of the effective charge transfer between Ag and the $SeZnO_3$ nanosheets and the higher conductivity of Ag, the nanocomposite showed an accelerated response/recovery rate. The demonstration of Ag/$SeZnO_3$-based pressure sensors can be helpful for the further improvement in the pressure sensing properties of materials.

Author contributions

The manuscript was written through the contributions of all authors. All authors have given approval for the final version of the manuscript.

Conflicts of interest

The authors declare no competing financial interest.

Acknowledgements

This work was supported by the National Key Basic Research Program of China (grant no.: 2021YFB3200302), the National Natural Science Foundation of China (grant no.: 51832001), the Fundamental Research Funds for the Central Universities of China, the Joint Research Funds of Department of Science & Technology of Shaanxi Province and Northwestern Polytechnical University (grant no.: 2020GXLH-Z-026 and 2020GXLH-Z-027).

 © 2024 The Author(s). Published by the Royal Society of Chemistry

Open Access Article. Published on 21 November 2023. Downloaded on 1/13/2026 2:05:29 AM.
This article is licensed under a Creative Commons Attribution-NonCommercial 3.0 Unported Licence.

Notes and references

1 S. Gong, W. Schwalb, Y. Wang, Y. Chen, Y. Tang, J. Si, B. Shirinzadeh and W. Cheng, *Nat. Commun.*, 2014, **5**, 3132.
2 J. Shi, Y. Dai, Y. Cheng, S. Xie, G. Li, Y. Liu, J. Wang, R. Zhang, N. Bai and M. Cai, *Sci. Adv.*, 2023, **9**, eadf8831.
3 S. Wang, W. Deng, T. Yang, G. Tian, D. Xiong, X. Xiao, H. Zhang, Y. Sun, Y. Ao and J. Huang, *Nano Res.*, 2023, **16**, 1330–1337.
4 S. Wang, W. Deng, T. Yang, Y. Ao, H. Zhang, G. Tian, L. Deng, H. Huang, J. Huang and B. Lan, *Adv. Funct. Mater.*, 2023, 2214503.
5 Z. Feng, Q. He, X. Wang, Y. Lin, J. Qiu, Y. Wu and J. Yang, *ACS Appl. Mater. Interfaces*, 2023, **15**, 6217–6227.
6 Y. Zhang, F. Shi, C. Zhang, X. Sheng, Y. Zhong, H. Chong, Z. Yang and C. Wang, *Chin. Chem. Lett.*, 2023, **34**, 107700.
7 J. Qin, L. J. Yin, Y. N. Hao, S. L. Zhong, D. L. Zhang, K. Bi, Y. X. Zhang, Y. Zhao and Z. M. Dang, *Adv. Mater.*, 2021, **33**, 2008267.
8 Z. Shen, C. Yang, C. Yao, Z. Liu, X. Huang, Z. Liu, J. Mo, H. Xu, G. He and J. Tao, *Mater. Horiz.*, 2023, **10**, 499–511.
9 R. Sheng, J. Mu, R. V. Chernozem, Y. R. Mukhortova, M. A. Surmeneva, I. O. Pariy, T. Ludwig, S. Mathur, C. Xu and R. Surmenev, *ACS Appl. Mater. Interfaces*, 2023, **15**, 3731–3743.
10 L. Cheng, X. Hao, G. Liu, W. Zhang, J. Cui, G. Zhang, Y. Yang and R. Wang, *Biosensors*, 2023, **13**, 131.
11 J. Zhang, M. Ahmadi, M. Serra, E. Jimenez-Pique, L. Llanes and G. Fargas, *Ceram. Int.*, 2023, **49**, 11579–11588.
12 H. Tao, J. Yin, Q. Zong, L. Zhao, D. Ergu, J. Ma, B. Wu and B. Ma, *J. Alloys Compd.*, 2023, **935**, 168142.
13 C. M. Magdalane, K. Kaviyarasu, J. J. Vijaya, B. Siddhardha and B. Jeyaraj, *J. Photochem. Photobiol., B*, 2016, **163**, 77–86.
14 Y. S. Kim, G.-H. Lee, M.-C. Sung and D.-W. Kim, *Chem. Eng. J.*, 2021, **406**, 126896.
15 S. Cabuk, *Philos. Mag.*, 2020, **100**, 601–618.
16 H. Zhang, D. Zhang, B. Zhang, D. Wang and M. Tang, *ACS Appl. Mater. Interfaces*, 2022, **14**, 48907–48916.
17 C. Sow, G. Mettela and G. U. Kulkarni, *Annu. Rev. Mater. Res.*, 2020, **50**, 345–370.
18 H. Wang, Z. Li, Z. Liu, J. Fu, T. Shan, X. Yang, Q. Lei, Y. Yang and D. Li, *J. Mater. Chem. C*, 2022, **10**, 1594–1605.
19 A. R. Chakhmouradian and P. M. Woodward, *Phys. Chem. Miner.*, 2014, **41**, 387–391.
20 R. Shi, Z. Lou, S. Chen and G. Shen, *Sci. China Mater.*, 2018, **61**, 1587–1595.
21 Z. Hou, S. Feng, P. Hei, T. Yang, Z. Ran, R. Zheng, X. Liao, C. Shu and J. Long, *J. Power Sources*, 2019, **441**, 227168.
22 G. D. Park, J. H. Hong, J. H. Choi, J. H. Lee, Y. S. Kim and Y. C. Kang, *Small*, 2019, **15**, 1901320.
23 B. Ju, H. J. Song, G.-H. Lee, M.-C. Sung and D.-W. Kim, *Energy Storage Mater.*, 2020, **24**, 594–601.
24 G. H. Lee, M. C. Sung, J. C. Kim, H. J. Song and D. W. Kim, *Adv. Energy Mater.*, 2018, **8**, 1801930.
25 Y. Liu, L. Yang, Q. Chen, Z. Wang, Z. Yang, J. Cao, X. Wang, H. Li and X. Huang, *Chem. – Eur. J.*, 2022, **28**, e202200298.
26 J. Huang, X. Tang, F. Wang, Z. Wang, Y. Niu and H. Wang, *Adv. Eng. Mater.*, 2022, **24**, 2101767.
27 Z. Shen, X. Zhu, C. Majidi and G. Gu, *Adv. Mater.*, 2021, **33**, 2102069.

© 2024 The Author(s). Published by the Royal Society of Chemistry